

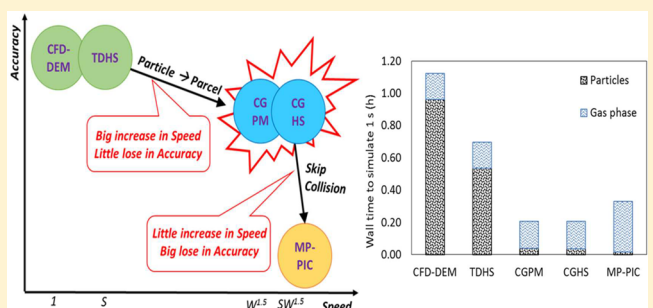
Assessment of Different Discrete Particle Methods Ability To Predict Gas-Particle Flow in a Small-Scale Fluidized Bed

Liqiang Lu,^{†,‡} Balaji Gopalan,^{†,‡} and Sofiane Benyahia*,[†]

[†]National Energy Technology Laboratory, Morgantown, West Virginia 26505, United States

[‡]West Virginia University Research Corporation, Morgantown, West Virginia 26505, United States

ABSTRACT: Several discrete particle methods exist in the open literature to simulate fluidized bed systems, such as discrete element method (DEM), time-driven hard sphere (TDHS), coarse-grained particle method (CGPM), coarse grained hard sphere (CGHS), and multiphase particle-in-cell (MP-PIC). The main difference between these methods is in the treatment of particle–particle interactions: by calculating collision forces (DEM and CGPM), using momentum conservation laws (TDHS and CGHS), or based on the particle stress model (MP-PIC). Here, these methods are compared by simulating the same small-scale fluidized bed with the same open-source code MFIX. The results indicate that both modeling the particle–particle collision by TDHS and lumping a few particles in a parcel increase the computation speed with little loss in accuracy. However, the MP-PIC method predicts an unphysical particle–particle overlap, which results in incorrect overall bed hydrodynamics. These results suggest using the CGHS method for fluidized bed simulations owing to its accuracy and efficiency.



1. INTRODUCTION

Fluidized bed technology has been widely used for many decades starting from Winkler's coal gasification in Germany and fluidized catalytic cracking in the United States.¹ However, the detailed hydrodynamics of fluidized beds is difficult to predict because the behavior of particles can range from solid-like to gas-like depending on the concentration and energy of the system. Thus, computer simulation has been widely used to understand and predict fluid–solids flow. Currently, there are mainly two types of simulations: Euler–Euler and Euler–Lagrange depending on the frame of reference used to solve the governing equations of motion. For the fluid phase, both approaches solve for the volume averaged Navier–Stokes equations in a fixed (Eulerian) frame of reference. The Euler–Euler approach considers particles as a continuum and solves for the volume averaged Navier–Stokes equations that are derived for both fluid and solids.² However, the Euler–Lagrange approach tracks the motion of each individual particles. Here a Lagrangian frame of reference moves with each particle simplifying the equations of motion to those stated by Newton's laws. The Euler–Euler approach is advantageous in computation speed but with some drawbacks such as numerical diffusion,³ constitution law for granular flow,⁴ and additional complexity such as particle size distribution.

The Euler–Lagrange approach avoids these drawbacks by simply tracking the movement of individual particles. The first Euler–Lagrange simulation of fluidized bed was performed by Tsuji et al.⁵ using a computation fluid dynamic coupled with discrete element method (CFD-DEM). In CFD-DEM, the

trajectory of every particle is tracked for all particle–particle collisions. The large computation cost of CFD-DEM is due to the tremendous number of particles and very small time steps required to capture the particle–particle collision process. To speed up the simulation, supercomputers and simplified models are usually used.^{6,7} There are many review papers on DEM in the open literature.^{8–10}

To reduce the computation cost, some model simplifications have been proposed along two directions. The first approach is to simplify the calculation of particle–particle interactions. In DEM, the time step needs to be 20 to 60 times smaller than total collision duration to numerically resolve the collision process. Instead of this soft-sphere method, the hard-sphere method handles the particle velocity directly based on momentum conservation during the collision. Hoomans et al.¹¹ simulated a bubbling fluidized bed using an event-driven hard-sphere model. Ouyang and Li¹² investigated gas–solids flow in a bubbling fluidized bed and CFB riser with a time-driven hard-sphere (TDHS) model. In the hard sphere simulation, a larger (compared to DEM) time step can be used especially in a TDHS in which particle overlaps can happen. However, in TDHS, there is still a need to search for particle–particle collisions. For the monodispersed system, the searching process can be accelerated by the linked-cell neighbor list method.

Received: June 7, 2017

Revised: June 8, 2017

Accepted: June 21, 2017

Published: June 21, 2017

However, for multidispersed systems with a large size ratio the efficiency will decrease dramatically, and therefore, more complex algorithms must be used to ensure higher efficiency. Multiphase particle-in-cell (MP-PIC)¹³ avoids the search of colliding particles by calculating particle–particle interactions based on a Eulerian particle stress model. Since there is no need to search for particle–particle collisions, even for multidispersed systems with large size ratio, the algorithm of MP-PIC maintains the same efficiency as for monodispersed systems. In MP-PIC and to reduce the cost of calculations, computation parcels lumping many particles W (W is larger than 1) are tracked instead of real particles. If coupled with DEM, it is usually called coarse grained particle method (CGPM);^{14,15} and if coupled with TDHS, it is called coarse grained hard sphere method (CGHS).¹⁶ The parcel based method reduces significantly the computation cost and has been used to simulate large-scale FCC riser,¹⁷ FCC regenerator,¹⁸ cyclones,¹⁹ circulating fluidized bed,^{20,21} liquid–solids leaching reactor,²² and heat transfer in bubbling fluidized bed.²³

On the basis of the different methods to handle particle–particle interactions and whether tracking real particles or computation parcels, the current Euler–Lagrange methods can be summarized in Figure 1.

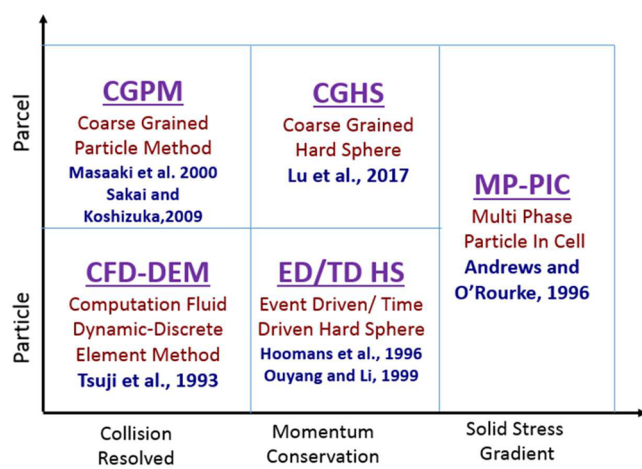


Figure 1. Euler–Lagrange simulation models based on methods to handle particle–particle interactions and the tracking of coarse or real particles.

Although these five methods were developed to simulate dense gas–solids flows and have been used by many researchers in the past, their computation speed and accuracy have never been compared directly with each other and with the same experimental data set. Thus, the purpose of this research is to provide a direct comparison of these five methods with each other and experiment data. To achieve this goal, the NREL Small-Scale Challenge Problem (SSCP-I, Gopalan et al (2016)) is simulated using the five methods described in Figure 1. All these models are implemented in one open-source multiphase flow simulation software (MFIX) in order to avoid the effect of using different flow solvers and fluid–solids coupling algorithms. The predictions of these different methods (such as pressure drop, solid velocity, and granular temperatures) are compared with publicly available experiment data and the computation speed is compared directly.

2. METHOD

In Euler–Lagrange simulation, the fluid phase is described as a continuum and governed by volume averaged Navier–Stokes equations, while the particles are tracked by Lagrange method and coupled with fluid phase on fixed Euler grids. The fluid flow equations were described previously²² and will not be repeated here.

2.1. Motion of Particles. For each particle, the momentum equation takes the form:

$$m_p \frac{dv_p}{dt} = F_{\text{external}} + F_{\text{inter-phase}} + F_{\text{p-p}} \quad (1)$$

$$I_p \frac{dw_p}{dt} = T \quad (2)$$

where m_p is the mass of the particle, the moment of inertia I is calculated by $m_p d_p^2 / 10$. On the right-hand side, the forces considered include the external forces such as gravity force, interphase forces such as pressure gradient force and drag force, and the particle–particle contact forces. For the Euler–Lagrange methods described in Figure 1, the difference in these models resides in the calculation of particle–particle forces.

For DEM, this force is calculated by assuming the particle–particle collisions as a linear spring-mass viscous damped system in normal and tangential directions. That is

$$F_{\text{pp}} = \sum_{j=1, j \neq i}^N (F_{ij}^n + F_{ij}^t) \quad (3)$$

$$T = \sum_{j=1, j \neq i}^N (L \mathbf{n} \times F_{ij}^t) \quad (4)$$

where F^n and F^t are collision forces in normal and tangential directions. L is the distance from particle center to contact point. The details of the DEM model can be found in the MFIX-DEM documentation,²⁴ and its verification and validation are also available in the literature.^{25,26}

For CGPM, the contact force is still calculated as in DEM by assuming all the real particles in the parcel can be arranged into a larger sphere with a diameter $d_p W^{1/3}$ where W is the number of real particles in a computation parcel. Then, the calculated force is divided by W to represent the force on a real particle:

$$F_{\text{pp}} = \sum_{j=1, j \neq i}^N (F_{ij}^n + F_{ij}^t) / W \quad (5)$$

$$T = \sum_{j=1, j \neq i}^N (L \mathbf{n} \times F_{ij}^t) / W^{5/3} \quad (6)$$

The details of the CGPM model and its validation can be found in a recent publication.²²

For MP-PIC, the motion of the solids phase is represented by discrete computational parcels and the particle–particle contact forces are modeled as the gradient of the solids phase pressure.

$$F_{\text{pp}} = -\frac{\pi d_p^3}{6 \epsilon_s} \nabla \tau \quad (7)$$

$$\tau = \frac{P_s \epsilon_s^\xi}{\max[\epsilon_{s, \text{cp}} - \epsilon_s, \epsilon(1 - \epsilon_s)]} \quad (8)$$

where P_s has units of pressure, and values between 1 and 100 Pa are recommended. $\epsilon_{s,CP}$ is the close packing limit. The constant ξ is also arbitrarily specified with recommended values in the range 2 to 5 (Auzerais et al., 1988). ϵ is a small number on the order of 10^{-7} and is added to remove the singularity at the close pack limit. Since the particle-particle force is directly applied at the center of the particles, the particle rotation is not considered in current MP-PIC. It is also difficult to physically explain the values of these parameters, and in current implementation in MFIX, it is used only as a guideline to decide the new velocity of a parcel approaching, exiting, or embedded in a close pack. The details of the implementation can be found in ref 27. The MFIX-PIC has been used to simulate liquid-solids fluidized bed²² and gas-solids riser.²⁸

For TDHS, the movement of particles in gas-solids flows is decomposed into suspension process and collision process. The suspension process accounts for external forces such as gravity and interphase forces while the collision process is handled by instantaneous binary collisions. For the suspension process, the velocities of particles are updated following Newton's law of motion:

$$m_p \frac{dv_p}{dt} = F_{\text{external}} + F_{\text{inter-phase}} \quad (9)$$

For collision processes, the velocities of particles are updated by instantaneous binary collisions. When particle i and j are in collision, the variation of momentum during impact is

$$\Delta P = -m_e(1 + e_n)v_n + J_t \quad (10)$$

$$J_t = -\max\left(\frac{2}{7}m_e(1 + e_t)|v_t|, \mu m_e(1 + e_n)|v_n|\right) \frac{v_t}{|v_t|} \quad (11)$$

where m_e is the effective colliding mass. e_n and e_t are normal and tangential restitution coefficients. J_t is the variation of momentum during impact in the tangential direction and μ is the sliding friction coefficient. Then, the velocity of particle i and j can be updated as

$$v_i = v_i - \frac{\Delta P}{m_i} \quad (12)$$

$$v_j = v_j + \frac{\Delta P}{m_j} \quad (13)$$

As for particle rotation, it can be calculated as

$$\omega_i = \omega_i - \frac{r_i n \times J_t}{I_i} \quad (14)$$

$$\omega_j = \omega_j - \frac{r_j n \times J_t}{I_j} \quad (15)$$

where I is the moment of inertia and is calculated by $m_p d_p^2 / 10$. The details of TDHS can be found in refs 12, and 29, and the extension to CGHS can be found in ref 16.

2.2. Interphase Forces. The interphase forces can be calculated as

$$F_{\text{interphase}} = \frac{\pi d_p^3}{6} \left(-\nabla P_f(x^i) + \frac{\beta_i}{1 - \epsilon_f} (v_f(x^i) - v_p^i) \right) \quad (16)$$

where $P_f(x^i)$ and $v_f(x^i)$ are the fluid pressure and velocity interpolated at particle i . β_i is drag coefficient of particle i . The

BVK³⁰ drag model derived from direct numerical simulation results is used in this paper. It can be calculated as

$$\beta = \frac{18\mu\epsilon_f(1 - \epsilon_f)}{d_p^2} F \quad (17)$$

$$F = \frac{10(1 - \epsilon_f)}{\epsilon_f^2} + \epsilon_f^2(1 + 1.5(1 - \epsilon_f)^{0.5}) + \frac{0.413Re_p}{24\epsilon_f^2} \left[\frac{\epsilon_f^{-1} + 3\epsilon_f(1 - \epsilon_f) + 8.4Re_p^{-0.343}}{1 + 10^{3(1-\epsilon_f)}Re_p^{-0.5-2(1-\epsilon_f)}} \right] \quad (18)$$

where

$$Re_p = \frac{\epsilon_f \rho_f |v_f - v_p| d_p}{\mu_f} \quad (19)$$

Here, the interphase forces are calculated based on the diameter of real particles. The assumption is that all the real particles in a parcel are subject to the same interphase drag force. In this research, the error induced by this assumption is small because the parcel size is small implying that the real particles are spatially close to each other. This error may become large as the parcel size increases due to differences in location of real particles in the center of the parcel and those in its outer layer. These issues have been discussed by Radl and Sundaresan,³¹ Ozel et al.³² and Lu et al.^{17,33} Since this research is focused on different collision models in addition to the fact that a small parcel size is used, the same drag model without further corrections is used in this research.

3. EXPERIMENT SETUP AND SIMULATION PARAMETERS

The experimental setup simulated in this study is shown in Figure 2. The pressure drop from 0.0413 to 0.3461 m is measured with Rosemount 1151DP Smart transmitters at 1 Hz frequency and Setra differential pressure transducers at 1 kHz. The solids

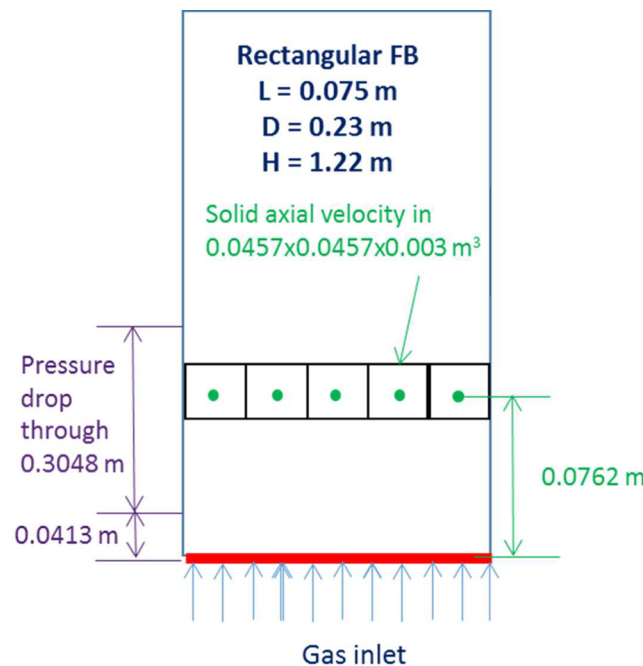


Figure 2. Pseudo-2D experiment device and measurement domain.

velocity is measured at 0.0762 m above the distributor using a high-speed particle image velocimetry system.³⁴ The detailed experiment description can be found in ref 35. A full technical drawing of the facility, including the distributor design, is available for download at <https://mfix.netl.doe.gov/experimentation/challenge-problems/>. The particle properties are listed in Table 1. It should be mentioned that there are

Table 1. Particle Properties

| parameter or property | value |
|--|-------------------|
| particle diameter, d_p (mm) | 3.256 |
| number of particles, N_p | 95 000 |
| parcel diameter, d_{parcel} (mm) | 6.512 |
| statistic weight, W | 8 |
| number of parcels, N_{parcel} | 11 875 |
| particle density, p_p (kg/m^3) | 1131 |
| spring constant, k_n (N/m) | 8.0×10^2 |
| particle–particle normal restitution coefficient, $e_{pp,n}$ | 0.84 |
| particle–particle tangential restitution coefficient, $e_{pp,t}$ | 0.84 |
| particle–wall normal restitution coefficient, $e_{pw,n}$ | 0.92 |
| particle–wall tangential restitution coefficient, $e_{pw,t}$ | 0.92 |
| particle–particle coefficient of friction, μ_{pp} | 0.35 |
| particle–wall coefficient of friction, μ_{pw} | 0.35 |

different approaches for scaling the properties of coarse grained parcels. Take for example the spring stiffness, Sakai et al.³⁶ scaled it by W (W is the number of real particles in a parcel), Chu et al.¹⁹ scaled it by $W^{2/3}$ times, Radl et al.³⁷ scaled it by $W^{1/3}$ times and Lu et al.¹⁷ used the same value as CFD-DEM. They derived these different laws based on different criteria. However, in gas–solids flow where the drag force has a dominant effect on the particle motion, this value has little influence on the results if set to a value large enough to avoid an unphysical overlap between colliding particles. Also, it should be mentioned that even for CFD-DEM simulations, a wide range of spring stiffness has been used in the open literature.³⁸ Thus, and to speed up the simulations conducted in this research, the same value of the spring stiffness constant is used in both CGPM and DEM. Furthermore, the same value of friction coefficient in CFD-DEM

was also used in CGPM. During the experiment, the superficial gas velocity is controlled at the following preset values: 2.19, 3.28, and 4.38 m/s. An ambient constant temperature at 20 °C was assumed, and air pressure was set at 101.325 KPa at the outlet. The simulation sets the same experimental values at inlet and outlet boundary while the nonslip boundary conditions are set at all walls in this 3D system. A uniform CFD grid of $16 \times 85 \times 4$ was set in each spatial direction (x,y,z) with the largest computational cell having a grid size of about 5 dp. This grid size has been used by Ayeni et al.³⁹ to simulate the same system. As indicated by many researchers, the grid size can influence the simulation results;^{33,40} however, the purpose of this research is to compare the influence of different collision models, while the grid size is kept the same for all simulations. If the grid size is too small, for coarse grained simulation there will be large numerical errors due to data mapping from Lagrangian point to Euler grid and vice versa. Note that the gravitational force is applied along the y -direction. The system is simulated for 60 s and data from the last 50 s are saved for further analysis at a frequency of 20 Hz.

4. RESULTS

In this section, several instant particle distributions and flow patterns are first compared. Then, the macroscale pressure drop is compared with experimental data. Next, the mesoscale solid velocity profile and granular temperature profile are analyzed. After that, particle–particle overlaps and particle voidage distributions are analyzed to explain the mesoscale and macroscale observations. Finally, the computation costs of these five methods are compared.

4.1. Instant Particle Distributions and Flow Patterns.

To visualize the differences in the fluidization behavior obtained with these five discrete methods, the instantaneous particle distribution and flow patterns are compared in this section. As shown in Figure 3, a large slugging bubble can be observed in the center of the fluidized bed for CFD-DEM (in Figure 3b–d), TDHS (in Figure 3a–d), CGPM (in Figure 3b,d), CGHS (in Figure 3a,c). The results obtained with these four methods also show that the particles in the center are moving upward while particles near the side walls are moving downward. Note that the

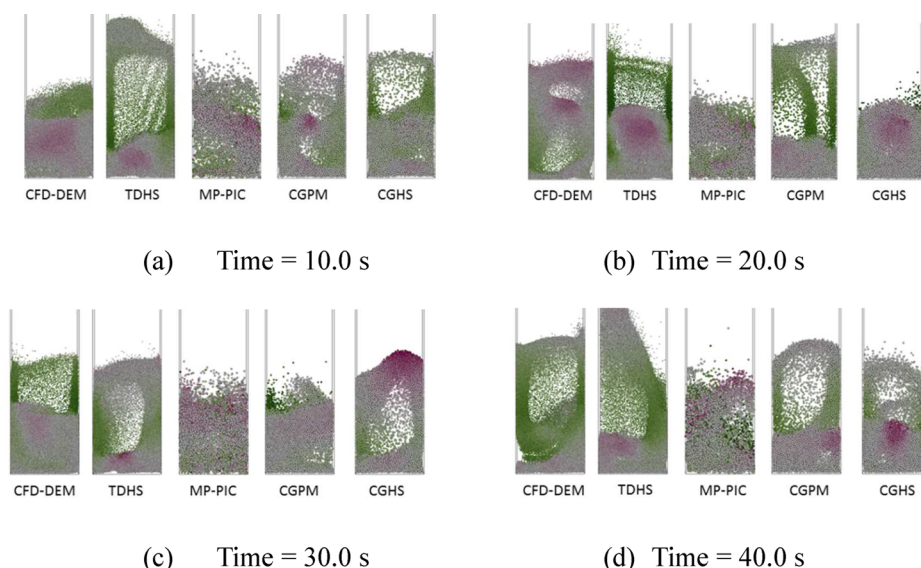


Figure 3. Instant particle distributions colored with vertical velocity component (purple, 2 m/s; green, -2 m/s) with different methods under an inlet velocity of 2.19 m/s.

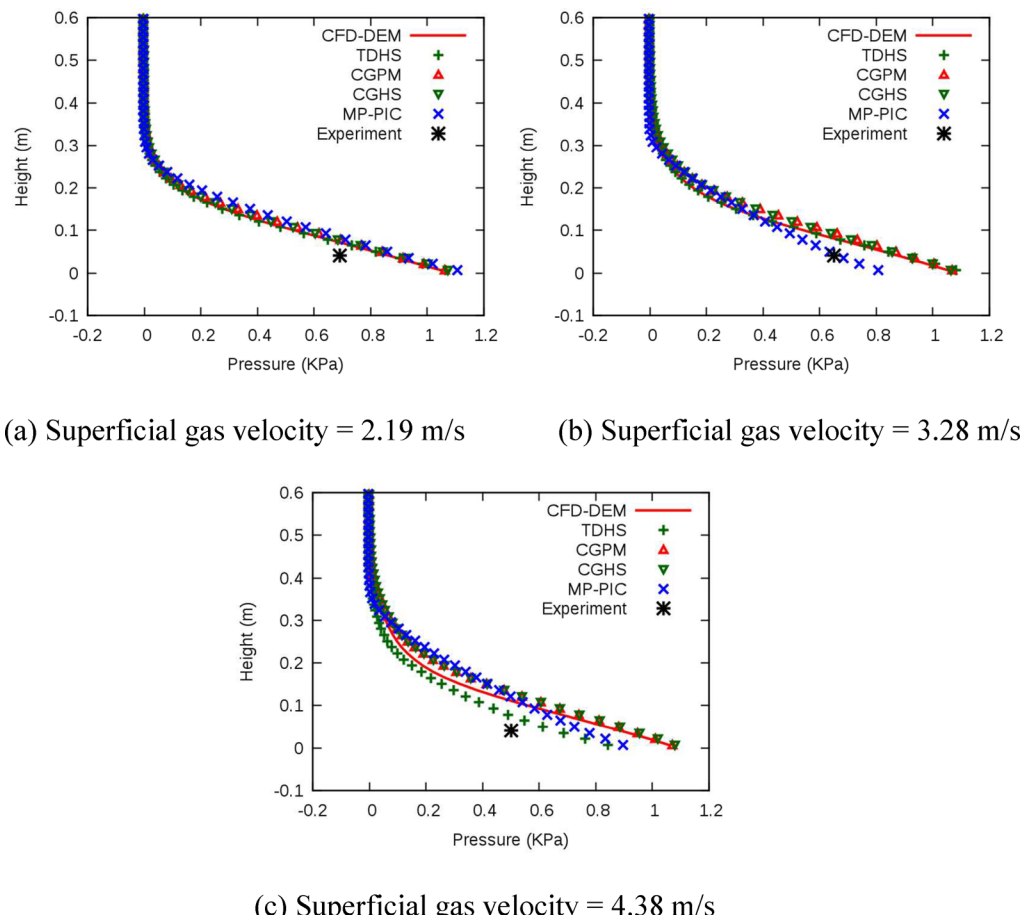


Figure 4. Pressure profile with different methods under different superficial gas velocities.

particles are colored with their upward velocity component. However, the results obtained with the MP-PIC method do not show any large slugging bubble in these four instants. The slugging phenomenon was rarely observed with MP-PIC for the whole simulation results stored at 20 Hz frequency for 60 s and totaling 1200 instant frames. Thus, it should be noted that although only 4 snapshots are shown in Figure 3, these represent typical flow behavior obtained from analyzing all the 1200 instant frames. Also, it should be noted that the core of the fluidized bed is more dilute than near the wall region, which is not as clearly shown with the MP-PIC method as it was with the other four methods.

The major difference between CFD-DEM/TDHS and CGPM/CGHS is in the assumption of lumping several real particles into a computation parcel to make these discrete simulations run faster. The similarity in the results of the overall fluidization behavior indicates that the main assumption of coarse-graining is reasonable even when the particle–particle collision process is hugely simplified to the binary parcel–parcel collision process. However, the difference in the results obtained with MP-PIC and the other four methods indicate that allowing particles to cross each other without interaction and ignoring particle rotation introduces significant uncertainties, which make it inaccurate for the simulation of Geldart D particles in a slugging bed. The results of these five methods will be quantitatively compared in the next section.

4.2. Pressure Drop. The pressure at two different heights is measured experimentally and provides a rough estimate of the bed weight and vertical particle distribution. The time-averaged

pressure profile is compared in Figure 4. It shows that all the five different methods result in a very similar pressure profile indicating that the pressure drop is not an ideal variable to assess the accuracy of different modeling or numerical approaches. Nevertheless, pressure data are easily collected experimentally and are used in this study because of their availability. The asterisk in the figure is the only experimentally measured pressure drop between 0.0413 and 0.3461 m with a frequency of 1 Hz for 300 s. In the simulation, the pressure data are analyzed with a frequency of 20 Hz for 50 s. Figure 4a shows that all the simulation results, obtained for inlet gas velocity of 2.19 m/s, overpredict the pressure drop by about 25%. When the gas velocity increased to 3.28 m/s, as shown in Figure 4b, still, all the simulations overpredict the pressure drop at the measurement point except for MP-PIC. The relative error is about 32%. Figure 4c shows the results obtained with an inlet gas velocity of 4.38 m/s. The relative error increases with increasing inlet gas velocity. This can be due to uncertainties in the drag model used in this study. There is still a debate among researchers on what drag correlations to use as indicated by the large body of work published in the literature on the effect of drag correlations on bed expansion height. However, this is beyond the scope of this current research that focuses on comparing the performances of different discrete methods.

We also noticed that, although the MP-PIC cannot capture the flow pattern as discussed in section 4.1. It can predict the pressure drop at the only experimental measurement point (note that we are not comparing a pressure profile). Again, this is because the pressure drop is only a rough estimate of the total

bed weight that is usually captured by models. The more interesting issue of bed expansion height was not addressed here as it was not measured experimentally. However, all models presented here show similar pressure drop profiles indicating similar bed height expansions, at least from a time-averaged perspective.

The Setra differential pressure transducers were used to measure the pressure drop fluctuation signals at a frequency of 1 kHz for 300 s. To keep consistent with simulation results, we also extracted data from the experimental measurements at a frequency of 20 Hz for 50 s. The spectrum of the pressure drop transient signals was analyzed using Fourier transform and are compared in Figure 5. The amplitude represents the

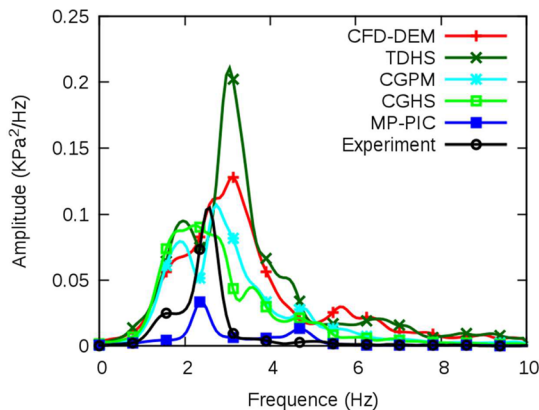


Figure 5. Power spectrum of the pressure drop fluctuation signals with different methods.

fluctuation energy, with a large value meaning the system is bubbling vigorously and a small value meaning the system is more homogeneous. The results show that CFD-DEM, CGPM, and CGHS predicted a similar amplitude profile compared with experimental data while the TDHS predicted a much higher and MP-PIC predicted a much lower amplitude profile. The lower amplitude in the power spectrum is another indication of less vigorous bubbling behavior as observed previously in Figure 3.

4.3. Solids Velocity Profile. The solids velocity is measured by a high-speed particle imaging technique (HSPIV). The depth of the field of view was approximately one particle diameter. From the field of view, five subsections of $0.0457\text{ m} \times 0.0457\text{ m} \times 0.003\text{ m}$

were extracted and analyzed. For a parcel based method such as CGPM or CGHS, the collision diameter of the parcel is 6.512 mm which is larger than the depth of the field of view of HSPIV. So, the sample volume is enlarged to include the whole depth of the bed that is $0.0457\text{ m} \times 0.0457\text{ m} \times 0.075\text{ m}$ for CGPM and CGHS. For MP-PIC, since the collision is not directly calculated both sample volumes are used.

Figure 6a compares the CFD-DEM, TDHS, and MP-PIC simulated solid vertical velocity in domain $0.0457\text{ m} \times 0.0457\text{ m} \times 0.003\text{ m}$ with experiment data. It shows that the CFD-DEM and TDHS can capture the profile correctly. This indicates that the hard-sphere method, which is computationally more efficient than the soft-sphere method, is accurate for simulation of a bubbling fluidized bed. However, further simplification, such as those assumed by the MP-PIC approach, lead to large errors as the predicted profile is flat near zero value in both qualitative and quantitative disagreement with experimental observations.

The horizontal solids velocity profile is compared in Figure 7. The particles in the left side of the fluidized beds have a positive horizontal velocity while the particles in the right side have a negative value. This indicates that all the particles are moving toward the center. This phenomenon is usually observed in the bubbling fluidized bed with core-annulus flow pattern and is also captured by the experiment data and simulation results of CFD-DEM and TDHS. However, the simulated horizontal velocity overpredicts the experiment data. For parcel based methods such as CGPM and CGHS, the predicted results are similar to those obtained by tracking real particles. Again, the MP-PIC method fails to capture the profile because of its failure to correctly capture the fluidization behavior of slugging as discussed in previous sections.

As shown in Figure 8, the predictive capability of all these numerical techniques diminishes as the superficial gas inlet velocity is increased to 3.28 and 4.38 m/s. It seems that the observed slugging regime becomes more difficult to predict with a simple drag model and particle–wall interactions. Koralkar and Bose⁴¹ compared the simulation results from six different drag models and concludes that it is difficult to select a single drag model to match all the studied cases. Ayeni et al.³⁹ proposed a new drag model which was claimed to reduce errors due to heterogeneous structures in fluidized beds. However, this research is only intended to compare the relative success of the different Euler–Lagrange methods in predicting the slugging

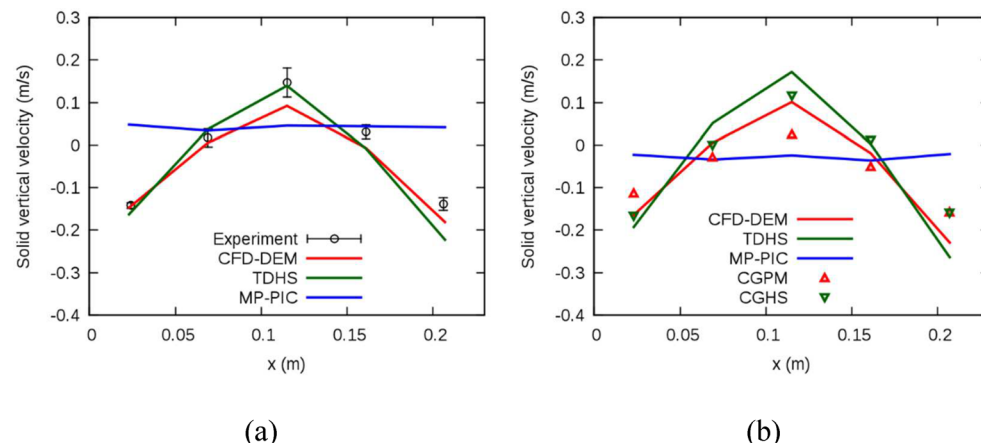


Figure 6. Radial profile of solid vertical velocity simulated with different methods under inlet velocity of 2.19 m/s: (a) sample domain is $0.0457\text{ m} \times 0.0457\text{ m} \times 0.003\text{ m}$; (b) sample domain is $0.0457\text{ m} \times 0.0457\text{ m} \times 0.075\text{ m}$.

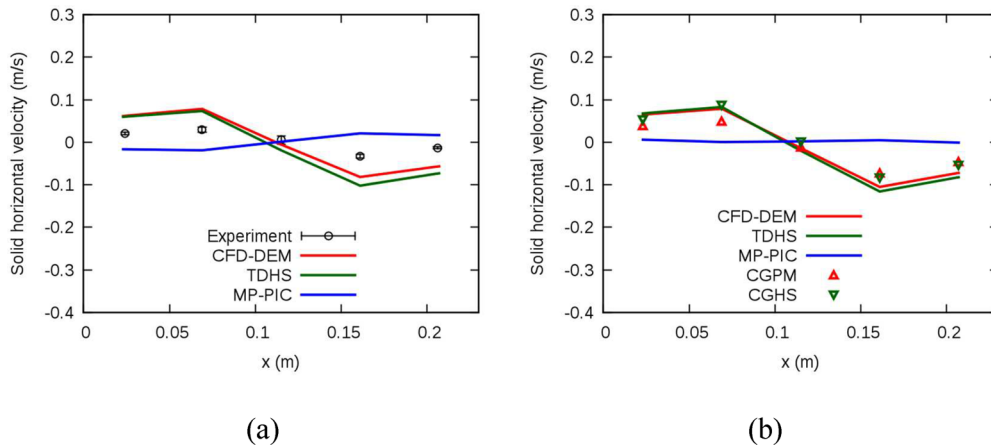


Figure 7. Radial profile of solid horizontal velocity simulated with different methods under inlet velocity of 2.19 m/s: (a) sample domain is 0.0457 m × 0.0457 m × 0.003 m; (b) sample domain is 0.0457 m × 0.0457 m × 0.075 m.

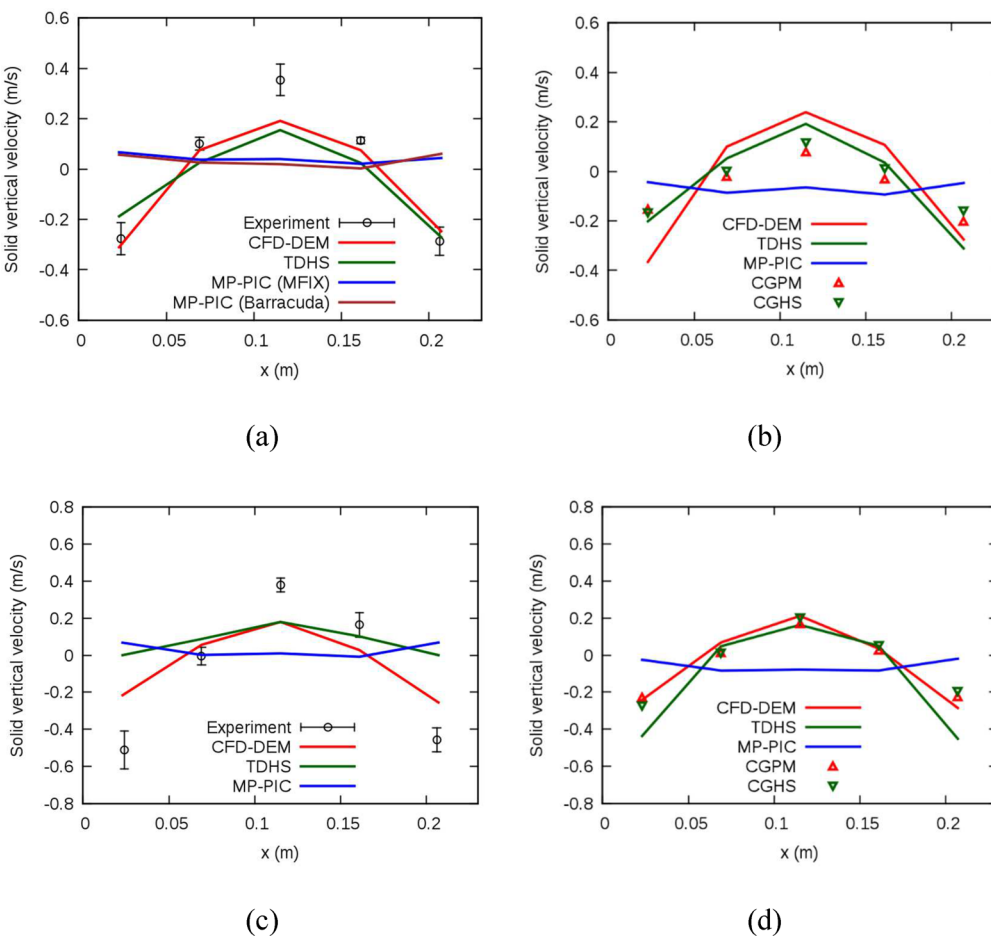


Figure 8. Radial profile of solid vertical velocity simulated with different methods: (a and b) inlet velocity is 3.28 m/s; (c and d) inlet velocity is 4.38 m/s; (a and c) sample domain is 0.0457 m × 0.0457 m × 0.003 m; (b and d) sample domain is 0.0457 m × 0.0457 m × 0.075 m.

regime of these type D particles. Although quantitative differences exist between the different discrete methods used in this study, the difference with the MP-PIC approach is qualitatively significant. For this reason, it was necessary to verify the validity of our MP-PIC results obtained with the MFIX code. Figure 8a includes a comparison of MP-PIC results obtained using both our open-source code MFIX and the commercial code Barracuda 17.0.4. The results show that our predictions using both software are nearly identical, which

removes doubts about the validity of our results. Previous studies⁴² conducted with MP-PIC have claimed some success in simulating large-scale reacting systems. However, it is impossible to prove the accuracy of the MP-PIC method at these large scales because conducting finer simulation, that is, DEM, is not yet possible. In this study, we report clear quantitative and qualitative disagreements for a small-scale system between MP-PIC and DEM results. Similar disagreements led previous researchers to conclude that the stress model in MP-PIC must be improved.⁴³ It

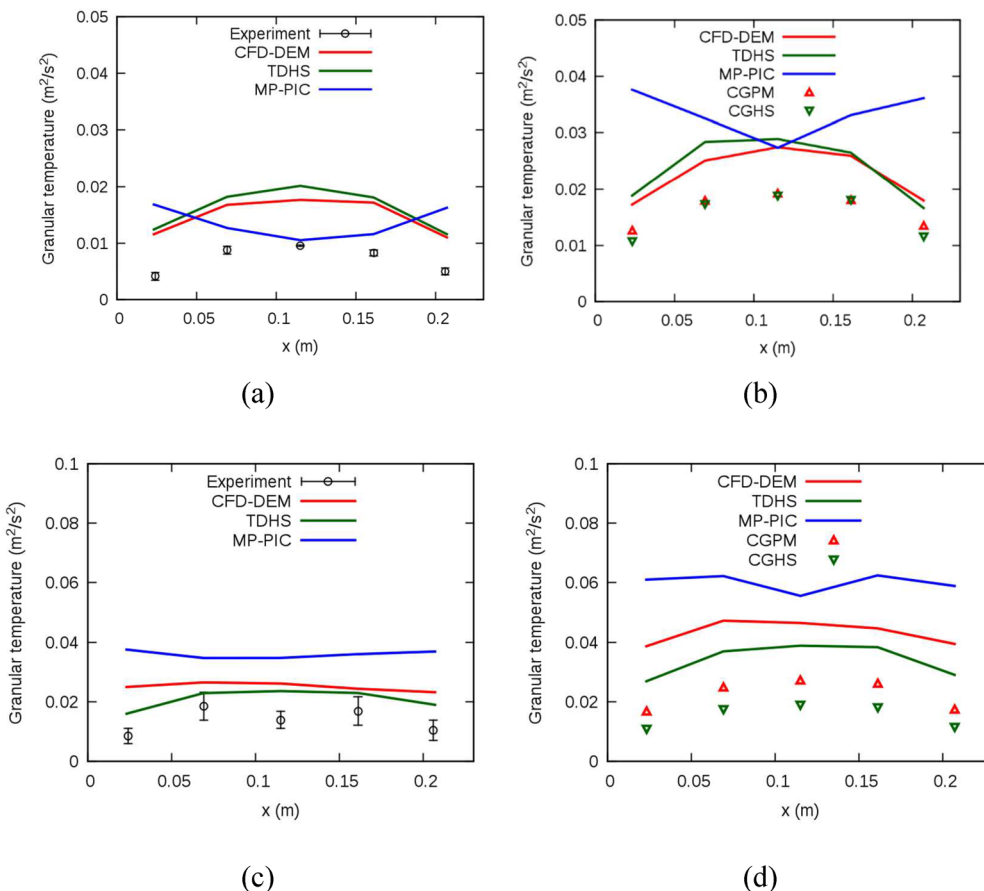


Figure 9. Granular temperature simulated with different methods: (a and b) inlet velocity is 3.28 m/s; (c and(d) inlet velocity is 4.38 m/s; (a and c) sample domain is 0.0457 m × 0.0457 m × 0.003 m; (b and d) sample domain is 0.0457 m × 0.0457 m × 0.075 m.

is possible to argue that MP-PIC requires a large amount of particles to make some statical sense in their continuum stress formulation. However, this argument is not physically sound because continuum models, such as TFM, have been applied with better success in simulating this same small system.⁴⁴ Therefore, this study suggest that researchers using the MP-PIC technique should be aware of these issues and focus more on validating and improving the MP-PIC technique as suggested by a previous study.⁴³

4.4. Granular Temperature. The previously analyzed time averaged pressure profile and solids velocity profile are first order statistics. To compare the simulation results with higher order statistics, the granular temperature profiles are compared in this section. Since the simulated system is a quasi-2D bed, the granular temperature is assumed to be zero in the depth direction. Thus, the granular temperature can be estimated as

$$\Theta = \frac{1}{3}(\Theta_x + \Theta_y) \quad (20)$$

$$\Theta_x = \frac{1}{N} \sum_{i=1}^N (v_x - \bar{v}_x)^2 \quad (21)$$

$$\Theta_y = \frac{1}{N} \sum_{i=1}^N (v_y - \bar{v}_y)^2 \quad (22)$$

As shown in Figure 9, the granular temperature has a parabolic profile for inlet gas velocity of 3.28 m/s, which flattens slightly as the velocity is increased to 4.38 m/s. Both the CFD-DEM and

TDHS simulation results overpredict quantitatively the granular temperature distribution in the bed. However, these methods qualitatively capture the shape of this distribution and its variation with inlet velocity. Again, the MP-PIC method fails to qualitatively capture the profile. For a parcel based method such as CGPM and CGHS, the computed granular temperature profiles are qualitatively like those predicted with real particle methods. The quantitative underprediction of the coarse-grained method occurs because the granular temperature is a measure of interparticle (interparcel) collisions as well as from the random velocity of the particles (parcels) themselves. However, the parcel based method reduces the agitation of particles in the system by lumping real particles into a large computation parcel. Therefore, the number of collisions in the system is reduced because the collisions between particles within the parcels are ignored. This will lead to a lower granular temperature (like the thermal temperature, the granular temperature is a measure of the agitation of particles).

According to our previous research,^{17,45} the underprediction of granular temperature can be reduced by lowering the value of restitution coefficient. However, in this case, only a small improvement can be observed even while the restitution coefficient is reduced to 0.1 as shown in Figure 10. Although the predicted granular temperature with smaller restitution coefficient is slightly larger than the uncorrected results, these predictions are still much lower than those obtained with CFD-DEM.

4.5. Particle Overlap and Voidage Distribution. The overlaps over colliding hard particles are naturally very small

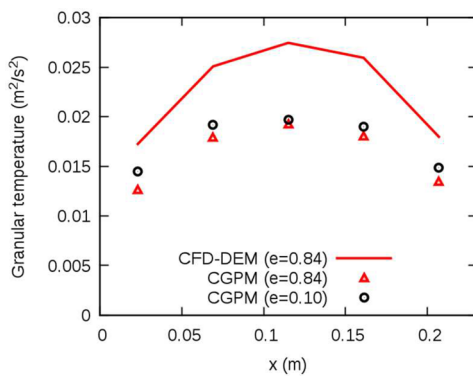
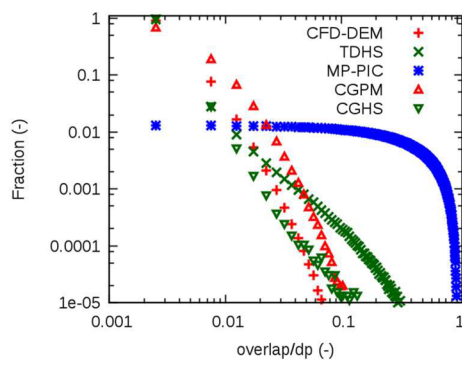


Figure 10. Granular temperature simulated with smaller restitution coefficient. Inlet velocity is 3.28 m/s with sample domain of 0.0457 m × 0.0457 m × 0.003 m.

relative to the particle diameter. However, and to speed-up the simulation, all of the methods investigated here allow some overlaps of colliding particles. The particle–particle overlaps will influence to some extent the void fraction, or voidage, distribution, and thus the hydrodynamics of the fluidized bed. The particle–particle overlaps are analyzed from 10 to 60 s with a frequency of 20 Hz and compared in Figure 11; note that the overlaps are normalized by particle or parcel diameter. It shows that CFD-DEM, TDHS, CGPM, and CGHS have a similar overlap distribution. For CFD-DEM, 90% and 97% of the particle–particle overlaps are smaller than 0.25% and 1% of the particle diameter, respectively. For TDHS and CGHS, the overlaps are even smaller than that in CFD-DEM. For CGPM, the overlaps are larger than CFD-DEM but still 87% of the overlaps are smaller than 1% of the particle diameter and 99% are smaller than 2.75% of the particle diameter. These relatively small overlaps introduce only a small error in the voidage calculation. The MP-PIC overlap distribution is constant for most overlaps of the order of particle diameter. This constant distribution is an indication of a random particulate flow that is insensitive to collisions. Particles will only “feel” the presence of each other at large overlaps where concentrations reach maximum packing and trigger a repulsive force to avoid the overcrowding of particles. The large overlaps predicted by MP-PIC will lead to unrealistic voidage distribution, which will result in incorrect magnitude of drag force, and finally predict unphysical fluidized bed dynamics.



(a) Overlap distribution

Figure 12 shows the voidage distribution of all computational cells from time 10 to 60 s and obtained with a frequency of 20 Hz.

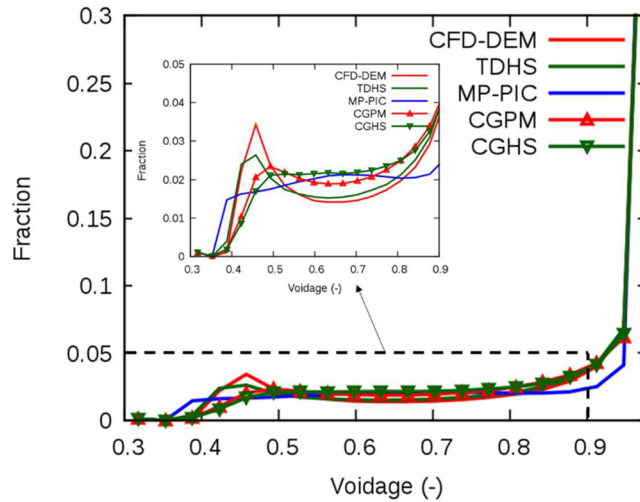
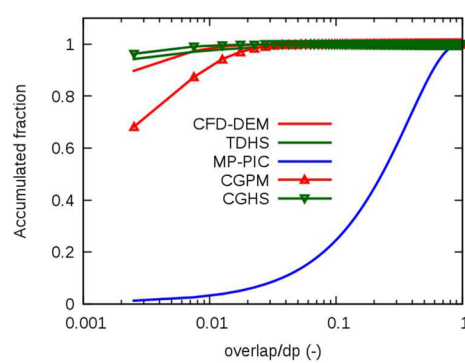


Figure 12. Voidage distribution with different methods obtained with inlet velocity of 2.19 m/s.

The higher fraction of cells with a voidage larger than 0.95 indicates the empty freeboard region of the fluidized bed. The results obtained with the MP-PIC technique show a statistically significant number of cells with void fraction below a value of 40%. However, and according to experiment data, the minimum fluidization voidage of the simulated particles is about 0.42. This smaller voidage simulated from MP-PIC is caused by the unphysical particle overlaps discussed in the previous paragraph. For particle based methods CFD-DEM and TDHS, there is a peak value at about 0.45. For parcel based methods such as CGPM, CGHS, and MP-PIC, the distribution is more flat in the voidage region from 0.5 to 0.8. This indicates that the parcel based method reduces the heterogeneity of the original system and is consistent with our previous analysis showing smaller granular temperature predicted by the parcel based method.

4.6. Computation Speed. For most discrete particle simulations, the main computation cost occurs in the particle solver and not in the fluid solver. This is due to the tracking of a large number of particles and the small time-steps needed to resolve collision processes. Thus, and as discussed in the introduction, many researchers try to reduce the computation



(b) Accumulated distribution

Figure 11. Particle–particle overlaps with different methods under an inlet velocity of 2.19 m/s.

cost either by reducing the number of particles or by increasing time steps. Using state of the art algorithms for particle–particle collision, the computation cost is $O(N)$, where N is the number of computation particles. For CFD-DEM, the time step is about 10 to 60 times smaller than collision duration which can be estimated as

$$t_c = \sqrt{\frac{m_{\text{eff}}}{k_n} (\pi^2 + (\ln e)^2)} \quad (23)$$

Thus, for a CFD-DEM simulation of N particles, the solid phase computation cost is about:

$$O(N)_{\text{CFD-DEM}} = a \left(\frac{S}{\sqrt{\frac{m_{\text{eff}}}{k_n} (\pi^2 + (\ln e)^2)}} \right) N + C \quad (24)$$

where a and C are constant values based on specific cases; S is the number of steps to resolve the collision duration. A typical value range of S is about 10 to 60.

CGPM with a statistic weight of W benefits from both the reduced number of particles and increased time steps and the corresponding computation cost is calculated as

$$O(N)_{\text{CGPM}} = \frac{1}{W^{1.5}} O(N)_{\text{CFD-DEM}} \quad (25)$$

For TDHS, the benefit of using a time-driven hard-sphere contact model is in avoiding resolution of the collision process leading to a larger solids time step. The time step for TDHS is determined by selecting the maximum allowed particle overlap. In this study, we assume the value of the maximum allowed particle overlap to be the same as that used in the CFD-DEM simulation. Thus, the time step can be as large as the collision duration derived from CFD-DEM. On the basis of this assumption, the computation cost of TDHS can be estimated as

$$O(N)_{\text{TDHS}} = \frac{1}{S} O(N)_{\text{CFD-DEM}} \quad (26)$$

For CGHS, the same criterion is used to estimate the solids time step with an additional benefit from reduced number of particles. Thus, the computation cost of CGHS can be estimated as

$$O(N)_{\text{TDHS}} = \frac{1}{SW^{1.5}} O(N)_{\text{CFD-DEM}} \quad (27)$$

For MP-PIC, the solid time step is limited by the CFL criteria, gas phase time step, and particle response time.²⁷ Thus, it is computed as

$$\begin{aligned} dt_{\text{MP-PIC}} \\ = \min \left\{ \min \left\{ \frac{\text{CFL} \times \Delta_i}{|V_{p,i}|}, i = 1, 2, 3 \right\}, dt_{\text{gas}}, \Delta_{\text{fac}} \tau_p \right\} \end{aligned} \quad (28)$$

where CFL and Δ_{fac} are user defined fractions; usually assumed less than 1. τ_p is particle response time and is calculated as

$$\tau_p = \frac{\rho_p d_p^2}{18\mu_g} \quad (29)$$

It is difficult to derive a relationship between time step of MP-PIC and DEM. However, and according to our experience and from published papers, the solids phase time step in MP-PIC is about 1–5 times smaller than the gas phase time step. Thus, and

for most cases, the time step of an MP-PIC simulation is much larger than that of a DEM. An MP-PIC simulation time also benefits from reduced number of particles as that in CGPM and CGHS.

The serial version of MFIX is used to directly compare the computation speed of these five methods. The wall time spent to simulate 1 physical second is compared in Figure 13 and shows

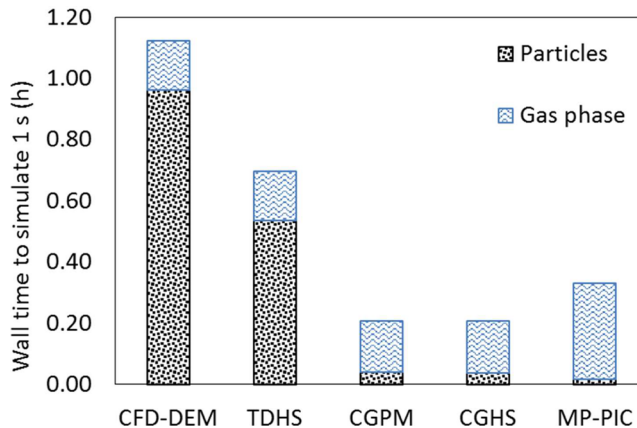


Figure 13. Computation speed of different methods using serial MFIX.

that the computation time of particles accounts for more than 85% of the total time for CFD-DEM. Here the particle computation time includes the calculation of drag force and solid pressure gradient in MP-PIC. The time spent in the gas-phase solver remains the same for CFD-DEM, TDHS, CGPM, and CGHS. However, the MP-PIC gas-phase solver is twice slower than other methods even though the same solver based on the SIMPLE algorithm is used for all these approaches. The only possible reason for this behavior is the different fluidized bed dynamics that are obtained with MP-PIC. For a particle solver, there is about 2 times the speedup of TDHS due to doubling the time step used. For a parcel based method such as CGPM and CGHS, the speedup is about 24 to 26 times because of the reduced number of particles and larger time step. There is also about another 2 times speedup of MP-PIC because it avoids calculation of the particle–particle collisions and thus benefits from a further simplified model and larger time step.

The previous comparison is based on serial version MFIX. However, modern computers comprise more than one CPU core, and many researchers have access to supercomputer clusters with hundreds to millions of CPU cores. For the larger scale fluidized bed, the CFD-DEM, TDHS, CGPM, and CGHS can benefit from the near linear-scale efficiency of distributed parallel computation. However, for MP-PIC only shared memory parallel is available in MFIX and according to our knowledge there is no MP-PIC software using parallel distributed memory. This study suggests that, for both small-scale and large-scale fluidized bed simulations, the CGHS method provides an overwhelmingly better accuracy than MP-PIC, and a speed of execution that rivals its nearest competitor.

5. CONCLUSIONS

In this research, a small-scale bubbling fluidized bed is simulated with five different Euler–Lagrange methods. As summarized in Figure 14, modeling the particle–particle collision process is accurately captured by TDHS with an increase in computation speed. Tracking lumped parcels will significantly increase the computation speed with little loss in accuracy. Ignoring the

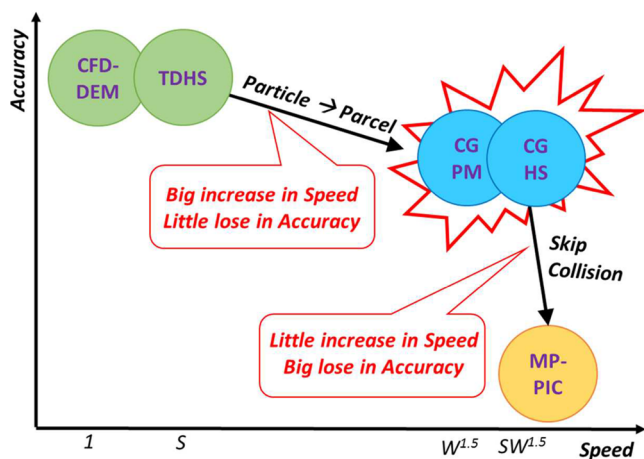


Figure 14. Accuracy and computation speed of different methods.

physics of collision, such as by MP-PIC leads to large loss in accuracy with a little gain in computation speed. This large loss in accuracy is attributed to unreasonable particle–particle overlaps that lead to unphysical fluidized bed hydrodynamics. The failure of MP-PIC in this particular system suggests that MP-PIC is not applicable for small systems with large particle size and the conclusion is consistent with other publications^{42,43} suggesting that the MP-PIC should be used to simulate a large-scale fluidized bed with large amounts of particles with small size. The computation cost of soft-sphere discrete particle simulation can be reduced largely by using CGHS, which benefits from a larger time step and a reduced number of computation particles. Additionally, we can say that a numerical solution obtained with CGHS will converge to that using DEM if the size of a parcel is reduced to that of a real particle and the physical time step of the hard-sphere contact method is also reduced to that of a soft-sphere. The same cannot be said for the MP-PIC method as a converged solution to that of DEM is not guaranteed and may, indeed, be impossible. Thus, we demonstrate in this study that coarse-grained models coupled with an improved time-driven hard-sphere contact algorithm can simulate fluidized bed processes inexpensively and accurately.

AUTHOR INFORMATION

Corresponding Author

*E-mail: sofiane.benyahia@netl.doe.gov.

ORCID

Liqiang Lu: [0000-0002-5101-1688](https://orcid.org/0000-0002-5101-1688)

Notes

This report was prepared as an account of work sponsored by an agency of the United States Government. Neither the United States Government nor any agency thereof, nor any of their employees, makes any warranty, express or implied, or assumes any legal liability or responsibility for the accuracy, completeness, or usefulness of any information, apparatus, product, or process disclosed, or represents that its use would not infringe privately owned rights. Reference herein to any specific commercial product, process, or service by trade name, trademark, manufacturer, or otherwise does not necessarily constitute or imply its endorsement, recommendation, or favoring by the United States Government or any agency thereof. The views and opinions of authors expressed herein do not necessarily state or reflect those of the United States Government or any agency thereof.

The authors declare no competing financial interest.

ACKNOWLEDGMENTS

This research was supported in part by an appointment to the National Energy Technology Laboratory Research Participation Program, sponsored by the U.S. Department of Energy and administered by the Oak Ridge Institute for Science and Education.

REFERENCES

- (1) Squires, A. M.; Kwaik, M.; Avidan, A. A. Fluid beds: at last, challenging two entrenched practices. *Science* **1985**, *230*, 1329–1338.
- (2) Anderson, T. B.; Jackson, R. Fluid Mechanical Description of Fluidized Beds. Equations of Motion. *Ind. Eng. Chem. Fundam.* **1967**, *6*, 527–539.
- (3) Guenther, C.; Syamlal, M. The effect of numerical diffusion on simulation of isolated bubbles in a gas–solid fluidized bed. *Powder Technol.* **2001**, *116*, 142–154.
- (4) Kennedy, D.; Norman, C. What don't we know? *Science* **2005**, *309*, 75–75.
- (5) Tsuji, Y.; Kawaguchi, T.; Tanaka, T. Discrete particle simulation of two-dimensional fluidized bed. *Powder Technol.* **1993**, *77*, 79–87.
- (6) Xu, J.; Qi, H. B.; Fang, X. J.; Lu, L. Q.; Ge, W.; Wang, X. W.; Xu, M.; Chen, F. G.; He, X. F.; Li, J. H. Quasi-real-time simulation of rotating drum using discrete element method with parallel GPU computing. *Particuology* **2011**, *9*, 446–450.
- (7) Ge, W.; Lu, L.; Liu, S.; Xu, J.; Chen, F.; Li, J. Multiscale Discrete Supercomputing - A Game Changer for Process Simulation? *Chem. Eng. Technol.* **2015**, *38*, 575–584.
- (8) Zhong, W.; Yu, A.; Zhou, G.; Xie, J.; Zhang, H. CFD simulation of dense particulate reaction system: Approaches, recent advances and applications. *Chem. Eng. Sci.* **2016**, *140*, 16–43.
- (9) Zhu, H.; Zhou, Z.; Yang, R.; Yu, A. Discrete particle simulation of particulate systems: A review of major applications and findings. *Chem. Eng. Sci.* **2008**, *63*, 5728–5770.
- (10) van der Hoef, M. A.; Annaland, M. V.; Deen, N. G.; Kuipers, J. A. M. Numerical simulation of dense gas–solid fluidized beds: A multiscale modeling strategy. *Annu. Rev. Fluid Mech.* **2008**, *40*, 47–70.
- (11) Hoomans, B. P. B.; Kuipers, J. A. M.; Briels, W. J.; van Swaaij, W. P. M. Discrete particle simulation of bubble and slug formation in a two-dimensional gas–fluidised bed: A hard-sphere approach. *Chem. Eng. Sci.* **1996**, *51*, 99–118.
- (12) Ouyang, J.; Li, J. Particle-motion-resolved discrete model for simulating gas–solid fluidization. *Chem. Eng. Sci.* **1999**, *54*, 2077–2083.
- (13) Andrews, M. J.; O'Rourke, P. J. The multiphase particle-in-cell (MP-PIC) method for dense particulate flows. *Int. J. Multiphase Flow* **1996**, *22*, 379–402.
- (14) Sakano, M.; Yaso, T.; Nakanishi, H. Numerical Simulation of Two-dimensional Fluidized Bed Using Discrete Element Method with Imaginary Sphere Model. *Jpn. J. Multiphase Flow* **2000**, *14*, 66–73.
- (15) Sakai, M.; Koshizuka, S. Large-scale discrete element modeling in pneumatic conveying. *Chem. Eng. Sci.* **2009**, *64*, 533–539.
- (16) Lu, L.; Li, T.; Benyahia, S. An efficient and reliable predictive method for fluidized bed simulation. *AIChE J.* **2017**, *15832*
DOI: [10.1002/aic.15832](https://doi.org/10.1002/aic.15832).
- (17) Lu, L.; Xu, J.; Ge, W.; Yue, Y.; Liu, X.; Li, J. EMMS based discrete particle method (EMMS-DPM) for simulation of gas–solid flows. *Chem. Eng. Sci.* **2014**, *120*, 67–87.
- (18) Tang, G.; Silaen, A.; Wu, B.; Fu, D.; Agnello-Dean, D.; Wilson, J.; Meng, Q.; Khanna, S.; Zhou, C. Q. Numerical study of a fluid catalytic cracking regenerator hydrodynamics. *Powder Technol.* **2017**, *305*, 662–672.
- (19) Chu, K.; Chen, J.; Yu, A. Applicability of a coarse-grained CFD–DEM model on dense medium cyclone. *Miner. Eng.* **2016**, *90*, 43–54.
- (20) Lu, L.; Xu, J.; Ge, W.; Gao, G.; Jiang, Y.; Zhao, M.; Liu, X.; Li, J. Computer virtual experiment on fluidized beds using a coarse-grained discrete particle method—EMMS-DPM. *Chem. Eng. Sci.* **2016**, *155*, 314–337.

- (21) Nikolopoulos, A.; Stroh, A.; Zeneli, M.; Alabaid, F.; Nikolopoulos, N.; Ströhle, J.; Karella, S.; Epple, B.; Grammelis, P. Numerical investigation and comparison of coarse grain CFD – DEM and TFM in the case of a 1 MWth fluidized bed carbonator simulation. *Chem. Eng. Sci.* **2017**, *163*, 189–205.
- (22) Lu, L.; Yoo, K.; Benyahia, S. Coarse-Grained-Particle Method for Simulation of Liquid–Solids Reacting Flows. *Ind. Eng. Chem. Res.* **2016**, *55*, 10477–10491.
- (23) Lu, L.; Morris, A.; Li, T.; Benyahia, S. Extension of a coarse grained particle method to simulate heat transfer in fluidized beds. *Int. J. Heat Mass Transfer* **2017**, *111*, 723–735.
- (24) Garg, R.; Galvin, J.; Li, T.; Pannala, S. Documentation of open-source MFIX-DEM software for gas–solids flows; NETL, 2012.
- (25) Garg, R.; Galvin, J.; Li, T.; Pannala, S. Open-source MFIX-DEM software for gas–solids flows: Part I—Verification studies. *Powder Technol.* **2012**, *220*, 122–137.
- (26) Li, T.; Garg, R.; Galvin, J.; Pannala, S. Open-source MFIX-DEM software for gas–solids flows: Part II — Validation studies. *Powder Technol.* **2012**, *220*, 138–150.
- (27) Garg, R.; Dietiker, J., *Documentation of Open-Source Mfix–pic Software for Gas-Solids Flows*. NETL, 2013.
- (28) Li, F.; Song, F. F.; Benyahia, S.; Wang, W.; Li, J. H. MP-PIC simulation of CFB riser with EMMS based drag model. *Chem. Eng. Sci.* **2012**, *82*, 104–113.
- (29) Helland, E.; Occelli, R.; Tadrist, L. Computational study of fluctuating motions and cluster structures in gas–particle flows. *Int. J. Multiphase Flow* **2002**, *28*, 199–223.
- (30) Beetstra, R.; van der Hoef, M. A.; Kuipers, J. A. M. Drag force of intermediate Reynolds number flow past mono- and bidisperse arrays of spheres. *AIChE J.* **2007**, *53*, 489–501.
- (31) Radl, S.; Sundaresan, S. A drag model for filtered Euler–Lagrange simulations of clustered gas–particle suspensions. *Chem. Eng. Sci.* **2014**, *117*, 416–425.
- (32) Ozel, A.; Kolehmainen, J.; Radl, S.; Sundaresan, S. Fluid and particle coarsening of drag force for discrete-parcel approach. *Chem. Eng. Sci.* **2016**, *155*, 258–267.
- (33) Lu, L.; Konan, A.; Benyahia, S. Influence of grid resolution, parcel size and drag models on bubbling fluidized bed simulation. *Chem. Eng. J.* **2017**, DOI: 10.1016/j.cej.2017.06.002.
- (34) Gopalan, B.; Shaffer, F. A new method for decomposition of high speed particle image velocimetry data. *Powder Technol.* **2012**, *220*, 164–171.
- (35) Gopalan, B.; Shahnam, M.; Panday, R.; Tucker, J.; Shaffer, F.; Shadle, L.; Mei, J.; Rogers, W.; Guenther, C.; Syamlal, M. Measurements of pressure drop and particle velocity in a pseudo 2-D rectangular bed with Geldart Group D particles. *Powder Technol.* **2016**, *291*, 299–310.
- (36) Sakai, M.; Abe, M.; Shigeto, Y.; Mizutani, S.; Takahashi, H.; Viré, A.; Percival, J. R.; Xiang, J.; Pain, C. C. Verification and validation of a coarse grain model of the DEM in a bubbling fluidized bed. *Chem. Eng. J.* **2014**, *244*, 33–43.
- (37) Radl, S.; Radeke, C.; Khinast, J. G.; Sundaresan, S. *Parcel based approach for the simulation of gas-particle flows*. 8th International Conference on CFD in Oil & Gas, Metallurgical and Process Industries, Trondheim, Norway, June 21–23, 2011.
- (38) Lommen, S.; Schott, D.; Lodewijks, G. DEM speedup: Stiffness effects on behavior of bulk material. *Particuology* **2014**, *12*, 107–112.
- (39) Ayeni, O. O.; Wu, C. L.; Nandakumar, K.; Joshi, J. B. Development and validation of a new drag law using mechanical energy balance approach for DEM–CFD simulation of gas–solid fluidized bed. *Chem. Eng. J.* **2016**, *302*, 395–405.
- (40) Wang, J.; van der Hoef, M. A.; Kuipers, J. A. M. Why the two-fluid model fails to predict the bed expansion characteristics of Geldart A particles in gas-fluidized beds: A tentative answer. *Chem. Eng. Sci.* **2009**, *64*, 622–625.
- (41) Koralkar, N. V.; Bose, M. Performance of drag models for simulation of fluidized beds with Geldart D particles. *Adv. Powder Technol.* **2016**, *27*, 2377–2398.
- (42) Kraft, S.; Kirnbauer, F.; Hofbauer, H. CFD simulations of an industrial-sized dual fluidized bed steam gasification system of biomass with 8 MW fuel input. *Appl. Energy* **2017**, *190*, 408–420.
- (43) Liang, Y.; Zhang, Y.; Li, T.; Lu, C. A critical validation study on CFD model in simulating gas–solid bubbling fluidized beds. *Powder Technol.* **2014**, *263*, 121–134.
- (44) Lungu, M.; Wang, H.; Wang, J.; Yang, Y.; Chen, F. Two-Fluid Model Simulations of the National Energy Technology Laboratory Bubbling Fluidized Bed Challenge Problem. *Ind. Eng. Chem. Res.* **2016**, *55*, 5063–5077.
- (45) Benyahia, S.; Galvin, J. E. Estimation of Numerical Errors Related to Some Basic Assumptions in Discrete Particle Methods. *Ind. Eng. Chem. Res.* **2010**, *49*, 10588–10605.